INTERNATIONAL JOURNAL OF HYDROGEN ENERGY 48 (2023) 723–739

Available online at www.sciencedirect.com

ScienceDirect

journal homepage: www.elsevier.com/locate/he

# High-pressure hydrogen permeability model for crystalline polymers

*Hiroyuki Kanesugi* [a,*], *Keiko Ohyama* [b], *Hirotada Fujiwara* [b], *Shin Nishimura* [a,b]

[a] *Department of Hydrogen Energy Systems, Graduate School of Engineering, Kyushu University, Japan*
[b] *Research Center for Hydrogen Industrial Use and Storage (HYDROGENIUS), Kyushu University 744 Motooka, Nishi-ku, Fukuoka, 819-0395, Japan*

## HIGHLIGHTS

- $H_2$ permeability of LDPE, HDPE, PA11 are measured under high pressure for two methods.
- New permeation model for crystalline polymers is developed in terms of the tortuosity.
- The results of pressure dependency of hydrogen permeability are reproduced by developed model.

## GRAPHICAL ABSTRACT

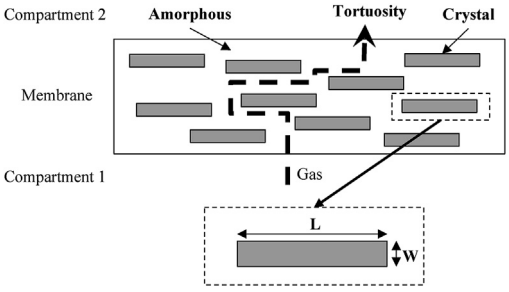


## ARTICLE INFO

*Article history:*
Received 21 May 2022
Received in revised form
20 September 2022
Accepted 21 September 2022
Available online 19 October 2022

*Keywords:*
Hydrogen gas permeation
Tortuosity
Crystallite
Amorphous
Free volume

## ABSTRACT

Molded seal devices made of crystalline polymers are widely used in high-pressure hydrogen equipment. A method for evaluating high-pressure hydrogen permeability was recently reported; however, the evaluation cost is extremely high. To select suitable crystalline polymers for molded hydrogen seals or barrier devices, a high-pressure hydrogen permeability prediction method using the polymer structure and its conventional properties is required.

In this study, we measured the pressure dependency of the hydrogen permeability of low-density polyethylene (LDPE), high-density polyethylene (HDPE), and polyamide 11 (PA11). We constructed the permeation model for crystalline polymers in terms of the tortuosity induced by their higher-order structures and free volume change in the amorphous region evaluated using PVT method for measuring the relationship between pressure ($p$), specific volume ($v$) and temperature ($T$) in the molten-solid state of a polymer. The results of the pressure dependency of hydrogen permeability were reproduced by the developed permeation model.



* *Corresponding author.*
E-mail address: hiroyuki.kanesugi.784@s.kyushu-u.ac.jp (H. Kanesugi).
https://doi.org/10.1016/j.ijhydene.2022.09.205

## Introduction

Concern about climate change is growing due to global warming. Carbon dioxide emissions due to energy consumption must be reduced as soon as possible. According to reports from the Ministry of Land, Infrastructure, Transport and Tourism of Japan based on the survey results [1] of the National Institute for Environmental Studies in Japan, carbon dioxide emissions from automobiles were about 16% of the total carbon dioxide emissions in 2019 [2]. Therefore, reducing carbon dioxide emissions in this sector is crucial and urgent. Following the introduction of commercial fuel cell electric vehicles (FCEVs), which do not emit carbon dioxide on the road, FCEV adoption has become a pressing issue.

Hydrogen fuel for FCEVs is incorporated as compressed hydrogen gas at 70 MPa due to the low volumetric energy density. The hydrogen fuel system of FCEV and hydrogen refueling station (HRS) comprise several components, including compressed hydrogen vessels and dispensing hoses, valves, filters, and nozzle–receptacle systems, which are equipped with hydrogen gas seal devices. The hydrogen dispensing systems at the HRS must withstand substantially higher pressures, which can approach 90 MPa.

We hope to contribute to the popularization of FCEV and HRS by improving the safety features of compressed hydrogen storage and transfer devices. The key components are type IV vessels and dispensing hoses, consisting of a polymeric inner layer and an outer reinforcing layer. The polymeric materials for the inner layer of these devices intrinsically have a permeability of compressed gases, including hydrogen gas, by a solution-diffusion mechanism [3]. Controlling the permeability by material design, especially the design of morphorogy and higher order structure of the polymeric materials is critical for minimizing fuel losses by the permeability of the polymeric materials for these devices.

Gas separation is an important application that uses permeability control technology by polymer material design. Purification of the mixed gases by removal of specific contaminant gas or extraction of the objective gas from the gas mixture due to the permeability difference of the gasous molecules which have different molecular dimensions is controlled by the gas separation polymer membrane design. In the case of hydrogen gas, contaminant gas with larger molecular dimension than hydrogen, such as methane, carbon dioxide, ammonia, nitrogen, etc., are separated by the polymer film with appropriate void volume controled by the higher order structure and the morphology [4]. As the material of the polymer film, there are many amorphous polymers, and studies have been reported such as perfluoropolymers, polyimides. As an example of perfluoropolymers, there are reports that methane is extracted from a mixed gas with high selectivity by using a copolymer that uses a monomer with a bulky branched structure for a part of the polymer [5,6]. In addition, as an example of polyimide, there is a report on the successful separation of methane with high selectivity by fabricating a membrane consisting of fibers with an asymmetrical hollow structure using polyimide with a bulky structure [7]. There is also a report of using polyimide containing a sensitizer and improving the selectivity by densifying the film structure with UV light [8]. Proton-exchange membranes (PEM) for fuel cells are applied the fuel hydrogen gas and air on each surface during cell operation. Gas barrier properties of PEM are important to ensure the efficiency of the fuel cell. Hydrogen permeability of several PEM, such as sulfonated tetrafluoroethylene-based fluoropolymers-copolymers, polystyrene sulfonic acid, were also reported [9,10].

In order to ensure the safety of compressed hydrogen storage and transfer device, it is necessary to ensure hydrogen barriers with a small molecular size using highly crystalline polymers, unlike gas separation membrane technology using amorphous polymers. Therefore, it is very important to focus on the morphology of crystalline polymers. Measurement data on the gas permeability of crystalline polymers have been reported by many researchers. Reported materials include polystyrene [11,12], low-density polyethylene [13,14], high-density polyethylene (HDPE) [15], polypropylene [16], polyvinylacetate [17], poly (methyl methacrylate) [18], polyamide 6 [19,20], polyvinyl alcohol [21], etc..

As examples of reports referring to crystalline polymer inner layers assuming compressed hydrogen storage and transfer equipment, there are some reports used polyethylene, polyamide 11 and ethylene vinyl alcohol copolymer for pipelines [22], inorganic component/PA6 composites for storage tank [23], amorphous polyvinyl alcohol for dispensing hoses [24]. The main points of the means to achieve the gas barrier in these reported examples are, firstly, to enhance the interaction of polymer molecular chains, and secondly, to use a polymer molding with high crystallinity and orientation to provide a path for gas diffusion. The third is to slow down gas diffusion by reducing the free volume of the polymer and bypassing the gas with fillers.

Several studies have previously been conducted to efficiently design materials considering polymer permeability. The technologies for predicting gas permeability required for the current material design have been constructed based on the basic chemical structure of polymers in the literature. Salame has extensively published the “permachor method” for predicting the permeability of barrier-type polymers to gases such as oxygen. The permachor parameters for a particular polymer are calculated from empirically derived coefficients for each chemical group within the polymer repeat unit [25]. Bicerano also considers polymer cohesive energy, packing, and rotational degrees of freedom in a Salame-like approach [26].

The application of the gas diffusion theory through the free volume in the polymer has also been reported. Lee suggests using a specific free volume defined as $v - v_0$ to correlate the free volume with the gas permeability coefficient of various polymers used in gas separation technology [27]. Park developed a more accurate scheme for predicting the permeability of six gases through over 100 rigid polymer by free volume extension [28]. Cohen-Turnbell's theory [29], which is an extension of Fujita's free volume theory [30], defines the relational expression between the diffusion coefficient and the fractional free volume (*FFV*). It was explained that the diffusion coefficient decreases as the *FFV* decreases.

The studies referring to the aforementioned gas permeability prediction do not address the hydrogen permeability

prediction in high-pressure environments, and it is unclear whether it can be applied in its current form. Fujiwara et al. developed a high-pressure hydrogen permeability method (HPHP) [31,32]. They designed and manufactured a device that can accurately measure the hydrogen permeability of polymeric materials in steady-state using the HPHP method and reported high-pressure hydrogen gas permeability up to 100 MPa for polyethylene with different crystallinities. They also measured the permeability of 6 polyethylene types using a thermal desorption analysis (TDA) method, which is a nonsteady-state measurement method in which the permeability is derived from the diffusion process when the sample is exposed to atmospheric pressure after exposure to high-pressure hydrogen. They showed that the permeation coefficients of the polyethylene measured using the HPHP method is smaller than those measured using the TDA method. The decrease in gas diffusion coefficient of the polyethylene measured using HPHP methods is due to a change in the degree of crystallinity and the free volume compression effect of hydrogen pressure. As aforementioned, a technology for measuring the hydrogen permeability of crystalline polymers under high-pressure conditions has been reported; however, the HPHP method has only just been developed and reported, and the evaluation cost is extremely high. The prediction method of HPHP using the polymer structure and its conventional properties is required to select suitable crystalline polymers for high-pressure hydrogen seals or barrier devices, such as the inner layers of a type IV tank or dispensing hoses.

This study establishes a method for predicting hydrogen permeability up to 100 MPa based on hydrogen permeability data at low pressure that can be measured using the conventional method.

## Theory

### *Basic theories of gas permeation*

Gas diffusion and permeation in polymer matrices were originally understood in terms of tortuosity. Tortuosity is a process in which gas penetrates the surface of polymer film and goes through it by bypassing the barriers in the film, such as fillers. However, the model does not describe hydrogen permeation through crystalline polymers in terms of their higher-order structures, which include crystalline and amorphous components. Michael et al. [33] reported a correlation between polyethylene crystallinity and gas permeability at 0.0006 and 0.1 MPa. However, only a few experimental examples demonstrate a relationship between gas permeability and higher-order structure.

Gas permeation through a polymer film can be investigated using a differential pressure method. A polymer film divides a test vessel into two compartments, compartment 1 and compartment 2. A penetrant gas is introduced into compartment 1, and the gas molecules penetrate the polymer film. The polymer film is saturated with penetrant gas molecules via diffusion. Finally, the penetrant gas is transferred from compartment 1 to compartment 2 through the polymer film. The ability of the gas to move through a polymer film is described by its permeability coefficient, which is the product of its solubility and diffusion coefficients.

### *Free volume theory*

The diffusivity of a polymer is governed by the relationship between the unoccupied volume in the polymer, referred to as "free volume," and the size of the penetrant gas molecules. Free volume is created by the thermal vibration of the polymer segments, known as micro-Brownian motion. In equation (1), the specific free volume ($v_F$) is the difference between the polymer's specific volume ($v$) and the van der Waals volume ($v_0$) of the polymer molecules, which is a specific occupied volume by polymer chain molecules in the bulk polymer.

$$v_F = v - v_0 \tag{1}$$

Bondi's atom group contribution method was used to estimate the van der Waals volume ($v_0$). The *FFV* is defined as the ratio of the free volume ($v_F$) to the specific volume ($v$), as shown in equation (2).

$$FFV = \frac{v_F}{v} = \frac{(v - v_o)}{v} \tag{2}$$

Fujita [30] proposed equation (3) based on the relationship between the *FFV* and the diffusion coefficient ($D$).

$$D = A_d RT exp\left(-\frac{B_d}{FFV}\right) \tag{3}$$

where $R$ is the gas constant, $T$ is the temperature, $A_d$ and $B_d$ are constants related to the shapes and sizes of the penetrant molecules. We explained that the diffusion coefficient increases as the free volume fraction increases.

### *Tortuosity*

The permeability of fillers, such as silica or many types of carbon materials, is lower than that of polymeric materials. To investigate the permeability of a polymer that contains a low permeable filler, Fig. 1 (a) shows that the penetrant gas molecules bypass the filler and traverse the polymer film. The length of the apparent transfer pathway, depicted as a broken line in Fig. 1 (a), exceeds the film's thickness.

### *Predicting the hydrogen permeability of crystalline polymers*

The crystalline regions in a polymer film are barrier components if the concept of tortuosity is applied to a crystalline polymer. For example, there are several types of commercially available polyethylene with different densities depending on the branching chain structure originating from their polymerization methods, such as low-density polyethylene (LDPE) and high-density polyethylene (HDPE). The degrees of crystallinity of the polymers cause the differences in density. The permeability coefficient of LDPE exceeds that of HDPE by about one digit [34]. In addition, the size and amount of the crystal region, which is a barrier component, depends on the molding method, such as injection molding, extrusion molding, and blow molding, and procedure, such as the cooling temperature rate after heat molding. Predicting hydrogen permeation through a crystalline polymer

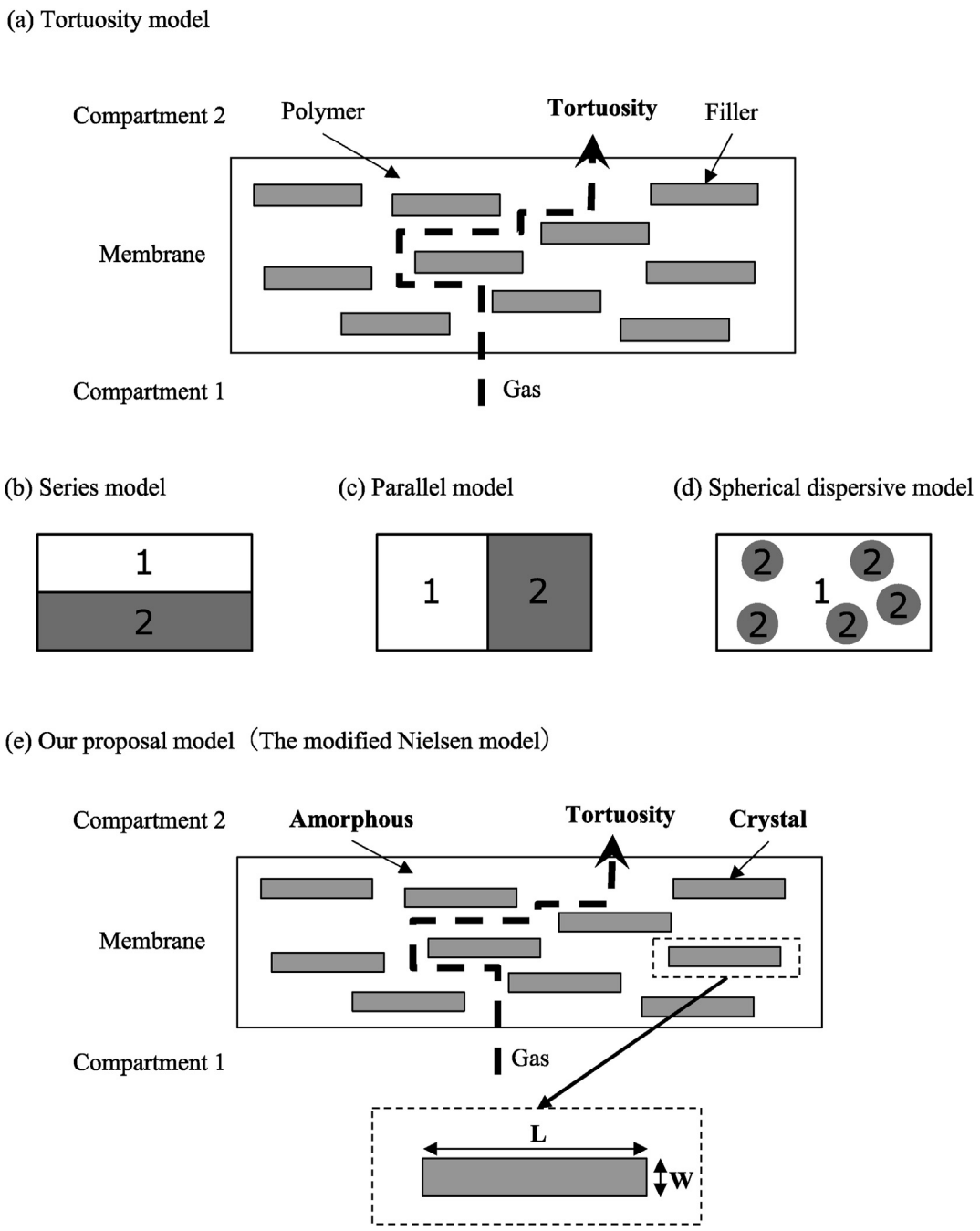


**Fig. 1 – Gas permeation model. (a) Tortuosity model, (b) series model, (c) parallel model, (d) spherical dispersion model, and (e) our proposed model.**

should be possible if quantitative information about the size and quantity of the crystalline components is available. In addition, considering the effect of the free volume compression of the crystalline and amorphous regions due to hydrostatic pressure is crucial when applying this concept to high-pressure hydrogen equipment. Predicting the hydrogen permeability of the inner layer material in a high-pressure hydrogen environment from the design stage of hydrogen equipment is possible if the two aforementioned points can be explained, and the development of hydrogen equipment is expected to be accelerated.

To predict the hydrogen permeability of a crystalline polymer, the higher-order structure of the polymer is assumed to be a binary system containing crystalline and amorphous regions.

A general theoretical model of gas permeation in a binary system is applied to the crystalline polymers. Several models describing the gas permeation coefficient of binary phase systems in terms of permeability coefficients and volume fraction of both phases were proposed, such as the series model in Fig. 1 (b) [35], parallel model in Fig. 1 (c) [35], and the spherical dispersive model in Fig. 1 (d) by Maxwell [36].

Nielsen [37] proposed a gas permeation model that considered the shape of the filler. Nielsen's model is often used to estimate the permeability of filled polymer systems when the filler is impermeable to the penetrant gas. When a gas permeates a polymer containing fillers, the gas permeates while bypassing the filler, resulting in a lower apparent permeability coefficient than when the polymer is unfilled. The relationship between these two permeation coefficients can be expressed by equation (4).

$$\frac{P_F}{P_U}=\frac{\varphi_P}{\tau} \tag{4}$$

where $P_F$ and $P_U$ are the permeation coefficients of filled and unfilled polymers, respectively. $\varphi_P$ is the polymer's volume fraction, and $\tau$ is the tortuosity factor. The tortuosity factor can be expressed by equation (5).

$$\tau = t_D/l \tag{5}$$

where $t_D$ is the distance traveled by a penetrant gas molecule through the polymer film and $l$ is the film thickness. The average morphology of filler particles is assumed to be disks or rectangular plates, which are oriented parallel to the polymer membrane surface. The tortuosity factor ($\tau$) can also be expressed by equation (6).

$$\tau = 1+\frac{L}{2W_F}\varphi_F \tag{6}$$

where $L_F$ and $W_F$ are the length and thickness of the filler, respectively, and $\varphi_F$ is the volume fraction of the filler. Equations (4) and (6) are combined for a cuboid filler. The ratio of the permeation coefficients of the filled and unfilled polymers is then expressed by equation (7).

$$\frac{P_F}{P_U}=\frac{1-\varphi_F}{1+\left(\frac{L_F}{2W_F}\right)\varphi_F} \tag{7}$$

This study proposes a method for predicting the high-pressure hydrogen permeation behavior of crystalline polymers using their morphology and low-pressure hydrogen permeability and other conventional properties. Thus, we focus on Nielsen's model to determine the permeation coefficient using the size and amount of filler to achieve this purpose. The crystallites in the crystalline polymers were assumed to be fillers uniformly distributed throughout the polymer matrix. The uniform polymer matrix was amorphous. The Nielsen model can be used to describe the effect of fillers on the gas permeability of filled polymers. According to the Nielsen model, the ratio of the permeability coefficients of filled and unfilled polymers is represented by equation (7). In this study, the Nielsen model (7) is modified for crystalline polymers considering higher-order structures of the crystalline polymers, as shown in Fig. 1(e). The permeation coefficient of the crystalline polymer is shown in equation (8).

$$\frac{P}{P_a}=\frac{1-\varphi_c}{1+\left(\frac{L_c}{2W_c}\right)\varphi_c} \tag{8}$$

where $P$ and $P_a$ are the permeation coefficients of the crystalline polymer and its amorphous region, respectively. $\varphi_c$ is the volume fraction of the crystallite. $L_c$ and $W_c$ are crystallite length and thickness, respectively. According to equation (8), the permeability of the crystalline polymer can be determined by the crystallite's shape factor, $L_c$ and $W_c$. The pressure dependency of the permeation coefficient of an amorphous region $P_a$, and $\varphi_c$, $L_c$, and $W_c$ of the crystallites are used to determine the permeability of crystalline polymer under high pressure.

The crystalline polymer is expected to be compressed under a high-pressure gas, such as hydrogen. Among higher-order structures, there are various studies on elastic modulus estimation and crystallite deformation under pressure. For example, the elastic modulus of the crystal region in polyethylene and polyvinyl alcohol is 235 GPa and 250 GPa, respectively [38]. The elastic modulus of the crystallites of the $\alpha$-type crystal of nylon 6 was determined by reflection in X-ray diffraction, which was discovered to be 157 GPa at room temperature [39]. At 90-MPa hydrogen, the compression in the crystallite's thickness direction is calculated to be less than 0.06%, which is negligibly small. Based on the results, this study assumes that the thickness, $L_c$, and width, $W_c$, of the crystallites are constant even under hydrostatic pressure.

Fujiwara et al. [31,32] confirmed the assumption concerning the higher-order structure of crystalline polymers under high-pressure gas for polyethylene series. Under these assumptions, the application of hydrogen pressure to the bulk crystalline polymer caused the amorphous region in the crystalline polymer to compress. Particularly, the free volume in the amorphous region is compressed. The diffusion coefficient of hydrogen in the amorphous region ($D_a$) under high pressure can be predicted using equation (3), which considers the diffusion coefficient measured at ambient pressure and the pressure dependency of FFV.

The following sections will detail the experimental verification of the concept for predicting HPHP from results obtained at ambient pressure.

## Experimental

### *Materials*

Low-density polyethylene (LDPE, UR951, Japanese polyethylene), high-density polyethylene (HDPE, HB111R, Japanese polyethylene), polyamide 12 (PA12, AESN TL, Alkema), polyamide 11 (PA11, BESN OTL, Alkema), and polyamide 6 (PA6, CM1041LO, Toray) were used as the crystalline polymers. Each material was put on a stainless mold, and a 300-μm-thick sheet specimen was obtained by compression molding using a 40-ton heat press machine manufactured by Toyo Seiki.

Vulcanized unfilled ethylene-propylene rubber (EPDM) was prepared as a reference for amorphous polyolefin material. The open roll-mixed composite of EPDM/dicumyl peroxide/stearic acid mixture (100/6/0.5 wt%) was vulcanized by hot press molding at 170 °C for 10 min, and a 300-μm-thick sheet specimen was obtained.

Table .1 shows the physical properties of each material. The measurement methods are described in the following sections.

**Table 1 – Physical properties of each sample at normal pressure.**

| Parameter | Hydrogen Permeability (0.6 MPa) | Heat fusion | Heat fusion 100% Crystal | Degree of crystalinity | Crystallite thickness | Crystallite length | Density |
|---|---|---|---|---|---|---|---|
| Symbol | $P^{0.6MPa}$ | $\Delta H$ | $\Delta H_0$ | $\chi_c$ | $W_c$ | $L_c$ | $\rho_{specimen}$ |
| Unit | $cm^3(STP) \cdot cm /(cm^2 \cdot s \cdot cmHg)]$ | J/g | J/g | – | nm | nm | $g/cm^3$ |
| EPDM | 5.00E-09 | | | | | | 0.8570 |
| LDPE | 9.12E-10 | 140.6 | 288.0 | 0.4882 | 8.30 | 4.60 | 0.9180 |
| HDPE | 4.34E-10 | 197.7 | 288.0 | 0.6865 | 8.30 | 14.96 | 0.9429 |
| PA12 | 2.60E-10 | 55.9 | 209.0 | 0.2673 | 4.30 | 2.80 | 0.9878 |
| PA11 | 2.10E-10 | 40.9 | 189.0 | 0.2164 | 1.70 | 2.68 | 1.0186 |
| PA6 | 4.36E-11 | 77.1 | 188.0 | 0.4101 | 2.60 | 2.46 | 1.1329 |

### *Differential scanning calorimetry*

The material's heat of fusion was determined using differential scanning calorimetry (DSC) QC2000 (TA Instruments) for 10 mg of a 300-μm-thick sheet specimen at a 5 °C/min temperature increase rate. Each material's degree of crystallinity, $\chi_C$, was determined as a ratio to the heat of fusion in its fully crystalline state. In addition, literature values of $\Delta H_0$ for perfect polyethylene crystals was 288 J/g [40], PA12, 209 J/g [41], PA11, 189 J/g [42] and PA6, 188 J/g [43] respectively.

### *Analysis of the higher-order structure*

(a) Wide-angle X-ray diffraction

$L_c$ was determined by Scherrer's equation (9) using a D8 Discover diffractometer (Bruker) to measure the obtained wide-angle X-ray scattering (WAXS) scattering profile of a 300-μm-thick sheet specimen. $\beta$ is the full width at half the maximum of the diffraction peak profile due to the small crystallite size in radians. $\theta$ is the Bragg angle, $K$ is the shape factor (0.9), and $\lambda$ is the X-ray wavelength.

$$L_c = K\lambda/\beta cos\theta \tag{9}$$

(b) Small-angle x-ray scattering

$W_c$ was measured using a Nano STAR SAXS instrument (Bruker) to measure the small-angle X-ray scattering (SAXS) scattering intensity of the sheet sample and estimate the distance between the lamella from the long period scattering. $W_c$ was determined using the Strobl analysis method with a one-dimensional electron-density correlation function equation [44]. The correlation function, $K(z)$, can be written as follows:

$$K(z) = (C_e(z) - C_e)(C_e(0) - C_e) = C_e(Z)C_e(0) - C_e^2 \tag{10}$$

where z is the direction normal to lamellar stacks, and the angular brackets indicate averaging over all coordinates, z, within a stack, which will pass through noncrystalline and crystalline layers. $C_e$ is the average electron density within the stack.

$K(z)$ can be obtained from the Fourier transform of the differential scattering cross-section $\Sigma(q)$.

$$\begin{aligned} K(z) &= \frac{1}{2r_e^2}\frac{1}{(2\pi)^3}\int_{-\infty}^{\infty} exp(iqz)4\pi q^2\Sigma(q)dq \\ &= \frac{1}{r_e^2}\frac{1}{(2\pi)^3}\int_{0}^{\infty} \cos(qz)4\pi q^2\Sigma(q)dq \end{aligned} \tag{11}$$

where $r_e$ is the classical electron radius, $q$ is the scattering vector ($q = (4\pi/\lambda)sin\,\theta$, where $\lambda$ is the wavelength of incident X-ray and $\theta$ is the Bragg angle).

### *Density*

The density of bulk polymer ($\rho_{specimen}$) was obtained by the underwater suspension method (JIS Z 8807–2012 compliant) using the electronic balance (Balance XSR225DUV, METLER TOLEDO). The solid is weighed in air ($A$) and then measured again in a replacement solution of known density ($B$). The density ($\rho_{specimen}$) of the solid was calculated equation (12). $A$ is the weight of the specimen in air, $B$ is the weight of specimen in the replacement solution, $\rho_0$ is the substituent density, and $\rho_L$ is the air density.

$$\rho_{specimen} = \frac{A}{A-B}(\rho_0 - \rho_L) + \rho_L \tag{12}$$

### *PVT method for measuring the relationship between pressure (p), specific volume (v) and temperature (T) in the molten-to-solid state of a polymer*

The relationship between the pressure, specific volume, and temperature in the resin's molten-to-solid state was measured. The relationship was measured using a PVT measuring device (GNOMIX Inc.). A cubic specimen (1 $cm^3$), whose weight and density were determined at atmospheric pressure and the temperature at the start of the experiment, was covered with a nickel cup. The specimen with the nickel cup was installed and sealed in a mercury-bath piezometer cell, with one end sealed with bellows. The volume conversion was estimated based on the change in the values of the bellows by heating and pressurizing the cell, and the density was obtained.

### *Hydrogen permeability measurement*

(a) Hydrogen permeation test under low pressure

The hydrogen permeation coefficient ($P^{0.6MPa}$) was determined using equation (13) by exposing 0.6 MPa hydrogen (≥99.999%, Suzuki Shokan) to a 300-μm-thick sheet sample using a differential pressure gas permeation tester (GTR-31A, GTR Tech). Q is the amount of permeable gas ($\mu L$), $l$ is the sample thickness, $\Delta p$ is the differential pressure, $A_{per}$ is the permeation area, and $t$ is time.

$$P^{0.6MPa} = \frac{(Q \times l)}{(\Delta p \times A_{per} \times t)} \tag{13}$$

(b) Measurement of hydrogen content and diffusion coefficient after hydrogen exposure using the TDA method, and calculation of the hydrogen coefficient under high-pressure conditions.

Disc specimens of 13-mm diameter were cut from each sample and exposed to a maximum of 90 MPa hydrogen gas at 30 °C for 24 h in a high-pressure vessel. The hydrogen release profile after decompression was measured using a thermal desorption analyzer (JSH-201, J-Science Lab Co., Ltd.). Gas chromatography was used to determine the amount of hydrogen released from the sample at 30 °C in argon flow every 5 min. The diffusion properties of hydrogen were estimated by fitting the data. The diffusion coefficient ($D$) and hydrogen content immediately after decompression ($C_0^H$; $t = 0$) were estimated by fitting equation (14) to the remaining specimen's hydrogen content using the least-squares method [45].

$$C_R^H(t) = \frac{32}{\pi} \cdot C_0^H \cdot \left[\sum_{n=0}^{\infty} \frac{exp\left\{-(2n+1)^2\pi^2 Dt \middle/ l_0^2\right\}}{(2n+1)^2}\right] \cdot \left[\sum_{n=1}^{\infty} \frac{exp\left\{-D\beta_n^2 t / r_0^2\right\}}{\beta_n^2}\right] \tag{14}$$

where $C_R^H$ (t) is the remaining hydrogen content at a given time (t), which is the time elapsed after decompression. $C_0^H$ is the hydrogen content at t = 0 per 1 g specimen, $D$ is the diffusion coefficient, $\beta_n$ is the root of the zero-order Bessel function, and $l$ and $r$ are the specimen's thickness and radius, respectively. The accuracy of TDA chromatography was used to determine the hydrogen content and diffusion coefficient, and the measurement error of specimens was calculated using the propagation of errors from equation (15).

Thereafter, the hydrogen permeation coefficient ($P_{TDA}$) was calculated under the high-pressure hydrogen conditions using equations (15)–(18) from the obtained hydrogen dissolution amount ($C_0^H$). $\rho_{Hydrogen}$ is the hydrogen density, $R$ is the gas constant, $T$ is the temperature, $p$ is the hydrogen pressure, $V_{Hydrogen}$ is the hydrogen volume per 1 $m^3$ specimen, $\upsilon_{specimen}$ is the specific volume determined by PVT measurement, and $D$ is the diffusion coefficient.

$$\rho_{Hydrogen} = M \times 10^{-3} \times p/RT \tag{15}$$

$$V_{Hydrogen} = C_0^H \times 10^{-3} \times \left(1 / \upsilon_{specimen}\right) / \rho_{Hydrogen} \tag{16}$$

$$S = V_{Hydrogen} / 0.0224 \times 101300 \tag{17}$$

$$P_{TDA} = S \times D \tag{18}$$

(c) High-pressure hydrogen gas permeation test (HPHP) under high-pressure conditions.

HPHP was conducted using high-pressure gas permeation cell equipment (Kouatsu system co., ltd., Saitaman, Japan) according to Fujiwara et al. [31,32]. Disk specimens of 27-mm diameter were sandwiched between sintered metal filters and set in a high-pressure cell for differential pressure transmission tests. The high-pressure cell and buffer tank in which hydrogen gas of target pressure is stored are connected with a shut-off valve. The interior of the cell and buffer tank was maintained at 30 °C, and the valve was opened when the test began, allowing hydrogen gas to be instantaneously supplied to one side of the specimen. The hydrogen gas pressure applied to one side of the test piece was constant, and the change in the amount of hydrogen permeating through the test piece with time was measured using gas chromatography to prepare an integrated transmission curve.

The amount of hydrogen permeated per unit time after reaching steady-state was measured, and the permeation coefficient was determined using equation (19).

$$P_{HPHP} = \frac{273.15 \times V \times l}{A_p \times \Delta p \times T \times 0.0227} \tag{19}$$

where $P_{HPHP}$ is the permeation coefficient, $l$ is specimen thickness, $V$ is the volume of hydrogen gas permeated to the low-pressure side at steady-state, $A_p$ is the permeation area, $\Delta p$ is the pressure difference, and $T$ is the temperature.

The diffusion coefficient ($D$) was determined using equation (20) based on the delay time ($\theta$) as follows:

$$D = \frac{l^2}{6\theta_{time}} \tag{20}$$

where D is the diffusion coefficient, $l$ is the thickness of the specimen, and $\theta_{time}$ indicates the delay time. The delay time ($\theta_{time}$) was determined by extrapolating the linear portion of the integrated transmission curve, when the hydrogen reaches steady-state, to the time axis.

The permeability coefficient ($P_{HPHP}$) is calculated by multiplying the solubility coefficient by the diffusion coefficient in the same way as in equation (19).

## Results and discussion

### *Pressure dependency of the hydrogen permeation and diffusion coefficients of LDPE, HDPE, and PA11*

The Pressure dependencies of three crystalline polymers, LDPE, HDPE, and PA11, were measured using the HPHP [31,32] and TDA methods [45]. Fig. 2 shows the results.

According to the results, the permeability coefficient of LDPE measured using the TDA method increases as the exposure hydrogen pressure rises. However, the results measured using the HPHP method decrease as the applied hydrogen pressure increases. The pressure dependency of the permeation coefficient measured using the TDA method was almost constant in the case of HDPE and PA11; however, the results measured using the HPHP method decreased as the applied hydrogen pressure increased. The aforementioned tendencies were also shown in the pressure dependencies of the diffusion coefficient for HDPE and PA11. The *FFV* controls the pressure dependence of the permeation and diffusion coefficient. Because the HPHP method is a steady-state measurement, hydrogen pressure was applied to the polymer films during the measurement. The free volume in the polymer film under high-pressure hydrogen is lower than that at atmospheric pressure. Therefore, the permeation and diffusion coefficients of these crystalline polymers decrease as the applied hydrogen pressure increases. In contrast, the parameters measured using the TDA method were determined by the hydrogen release profiles from the hydrogen-saturated specimens under atmospheric pressure. The specimens were free from static pressure following decompression of hydrogen exposure pressure, thus the free volume of the polymers after hydrogen exposure is equal despite their hydrogen exposure pressure. In the case of LDPE, the decompression process from the high exposure pressure may damage the specimen, and this damage can impact the hydrogen release profile and fitting result. The observed behavior, including PA11, is consistent with the results of LDPE and HDPE reported by Fujiwara et al. [31,32].

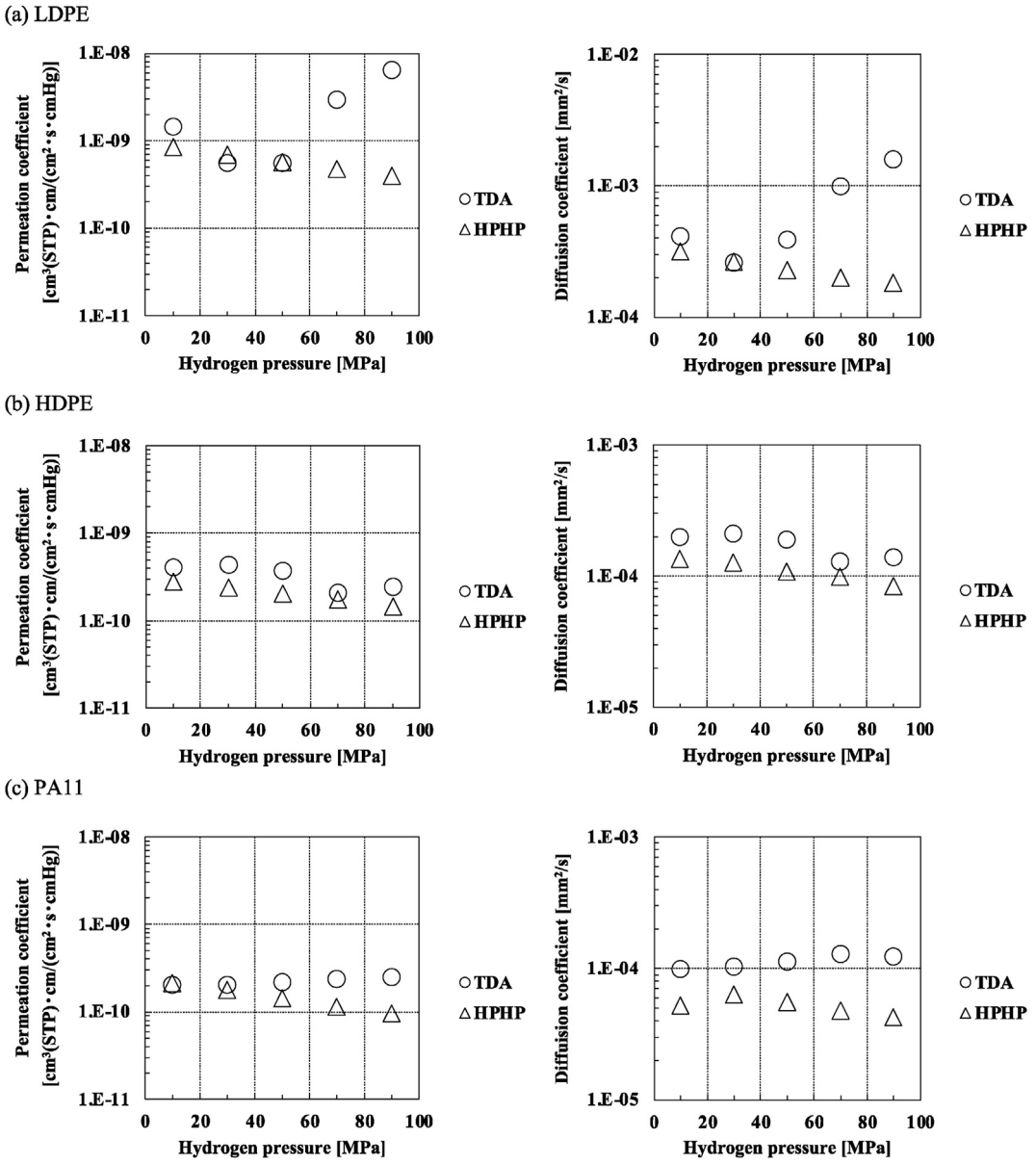


**Fig. 2 – Pressure dependency of the hydrogen permeation coefficient of crystalline polymers measured using the TDA and HPHP method. (a) LDPE, (b) HDPE, (c) PA11.**

To design high-pressure hydrogen equipment, it is crucial to know the hydrogen permeation properties at the equipment's operating hydrogen pressure. The model, which quantitatively describes high-pressure hydrogen permeation and diffusion coefficients, will be developed based on the aforementioned hydrogen permeation behavior.

### *Determination of the crystallite volume fraction, $\varphi_c$, for the tested polymers*

The membrane's crystallite content ($\varphi_c$) was calculated using equation (21). $V_c$ and $V$ are the crystallite and bulk polymer volumes, respectively.

$$\varphi_c = \frac{V_c}{V} \tag{21}$$

Volume can be calculated by dividing weight by density, as presented in equation (22). $m_c$ and $m$ are the weights of crystallite and bulk polymer; $\rho_c$ and $\rho$ are their densities, respectively.

$$\varphi_C = \frac{m_c \times \rho}{m \times \rho_C} \tag{22}$$

The degree of crystallinity ($\chi_c$) can be expressed as the ratio of the crystallite component to the polymer weight, as in equation (23).

$$\chi_c = \frac{m_c}{m} \tag{23}$$

Therefore, $\varphi_c$ can be expressed as equation (24).

$$\varphi_c = \chi_C \times \frac{\rho}{\rho_c} \tag{24}$$

Equation (24) shows that the degree of crystallinity, polymer density, and crystallite density are required to derive the volume fraction of the crystal. Table 1 summarizes the specimen's degrees of crystallinity. Table 2 shows each specimen's estimated crystallite volume fraction, $\varphi_c$.

### *Relationship between gas permeability ($P_a$) and fractional free volume ($FFV_a$) in amorphous regions at 0.6 MPa*

Penetrant gas molecules permeate the bulk crystalline polymer, bypassing the crystallites.

The amorphous region is the permeation pass. Section 2.2 shows that the diffusion coefficient is determined by the *FFV*. Permeability, which is the product of solubility and diffusivity, is also controlled by *FFV*.

The occupied volume, which is the van der Waals volume ($v_0$) in the bulk polymer obtained from its molecular structure, and the specific volume of a bulk polymer can be used to calculate *FFV*. Equation (25) shows that the occupied molar volumes of the polymers were estimated from the sum of the Bondi atomic group contributions ($v_{wi}$). Table 3 lists the $v_{wi}$ values. The molecular weights of the repeating polymeric units ($m_0$) were calculated using equation (26) and Table 3 shows the contribution parameter ($m_i$) of each functional group.

$$v_0 = \sum v_{wi} \tag{25}$$

$$m_0 = \sum m_i \tag{26}$$

The occupied density ($\rho_{occupied}$) is calculated using equation (27). The occupied volume fraction (k) is defined as the ratio of the density of bulk polymer ($\rho_{specimen}$) and occupied density ($\rho_{occupied}$), as seen in equation (28). The *FFV*, which is the "unoccupied volume" in the bulk polymer, is estimated as $1 - k$, s seen in equation (29). Table 4 summarizes the estimated results for EPDM, LDPE, HDPE, PA12, PA11, and PA6.

$$\rho_{occupied} = m_0 / v_o \tag{27}$$

$$k = \rho_{specimen} / \rho_{occupied} \tag{28}$$

$$FFV = 1 - k \tag{29}$$

**Table 3 – Mass ($m_i$) and the occupied molar volume ($v_{wi}$) of molecular functional group.**

| Parameter | Mass | Occupied molar volume |
|---|---|---|
| Symbol | $m_i$ | $v_{wi}$ |
| Unit | g/mol | $cm^3$/mol |
| $-CH_3$ | 15.0 | 13.7 |
| $-CH_2-$ | 14.0 | 10.2 |
| $-CH(CH_3)-$ | 28.1 | 20.5 |
| >C=CH- | 25.0 | 13.5 |
| -CH< | 13.0 | 6.8 |
| >C=O | 28.0 | 8.5 |
| -NH- | 15.0 | 4.0 |

**Table 2 – Crystallite volume fraction, $\varphi_c$, of each sample at normal pressure.**

| Parameter | Degree of crystalinity | Specimen density | Crystallite density | Crystallite volume fraction |
|---|---|---|---|---|
| Symbol | $\chi_C$ | $\rho_{specimen}$ | $\rho_C$ | $\varphi_C$ |
| Unit | – | $g/cm^3$ | $g/cm^3$ | – |
| EPDM | | 0.8570 | | |
| LDPE | 0.4882 | 0.9180 | 1.000 | 0.4482 |
| HDPE | 0.6865 | 0.9429 | 1.000 | 0.6473 |
| PA12 | 0.2673 | 0.9878 | 1.150 | 0.2296 |
| PA11 | 0.2164 | 1.0186 | 1.120 | 0.1968 |
| PA6 | 0.4101 | 1.1329 | 1.230 | 0.3777 |

**Table 4 – Fractional free volume in each crystalline polymer.**

| Parameter | molecular weights of repeating polymeric units | van der Waals volume | occupied density | the density of bulk polymer | occupied volume fraction | unoccupied volume fraction |
|---|---|---|---|---|---|---|
| Symbol | $m_0$ | $v_0$ | $\rho_{occupied}$ | $\rho_{specimen}$ | k | FFV |
| Unit | g/mol | $cm^3/mol$ | $g/cm^3$ | $g/cm^3$ | – | – |
| EPDM | 190.3 | 126.0 | 1.511 | 0.8570 | 0.5673 | 0.433 |
| LDPE | 28.0 | 20.5 | 1.370 | 0.9180 | 0.6698 | 0.330 |
| HDPE | 28.0 | 20.5 | 1.370 | 0.9429 | 0.6880 | 0.312 |
| PA12 | 197.3 | 125.0 | 1.578 | 0.9878 | 0.6261 | 0.374 |
| PA11 | 198.3 | 128.5 | 1.543 | 1.0186 | 0.6600 | 0.340 |
| PA6 | 128.2 | 77.3 | 1.658 | 1.1329 | 0.6835 | 0.317 |

The FFV represents the ratio of the free volume in the bulk crystalline polymer; however, to reduce hydrogen permeability under high-pressure gas conditions, the compression of the free volume part in the amorphous region, denoted as $FFV_a$, must be calculated. $FFV_a$ can be obtained from the ratio of van der Waals volume and specific volume as the "unoccupied space" in the amorphous region, which are the molecular chain motion region in the amorphous region.

The fractional free volume ($FFV_a$) is defined as the ratio of the free volume ($v_{Fa}$) to the specific volume ($v_a$), as shown in equation (30) in the amorphous region.

$$FFV_a = \frac{v_{Fa}}{v_a} = \frac{(v_a - v_o)}{v_a} \tag{30}$$

The density of the amorphous region ($\rho_a$) was calculated by substituting the volume fraction of the crystallinity in the crystalline polymer ($\varphi_c$) and the density of the crystallite ($\rho_c$) into equation (31). To obtain the specific volume ($v_a$) of the amorphous region, the density of the amorphous region ($\rho_a$) may be obtained from the volume fraction of crystallite ($\varphi_c$) and the density ($\rho_c$) of the crystalline region according to [46], and the reciprocal conversion can be performed using equation (32). Table 5 shows $\rho_a$, $v_a$, and $FFV_a$ of each sample obtained using equations (31) and (33).

$$\varphi_C = \frac{\rho - \rho_a}{\rho_c - \rho_a} \tag{31}$$

$$v_a = \frac{1}{\rho_a} \tag{32}$$

**Table 5 – Fractional free volume of the amorphous region ($FFV_a$) in each crystalline polymer.**

| Parameter | Amorphous Density | Amorphous specific volume | Amorphous free volume |
|---|---|---|---|
| Symbol | $\rho_a$ | $v_a$ | $FFV_a$ |
| Unit | $g/cm^3$ | $cm^3/g$ | – |
| EPDM | 0.8570 | 1.1669 | 0.4327 |
| LDPE | 0.8514 | 1.1745 | 0.3788 |
| HDPE | 0.8381 | 1.1931 | 0.3884 |
| PA12 | 0.9395 | 1.0644 | 0.4045 |
| PA11 | 0.9938 | 1.0063 | 0.3561 |
| PA6 | 1.0740 | 0.9311 | 0.3521 |

### *Predicting the hydrogen permeability coefficient in a high-pressure environment*

The diffusion coefficient ($D$) is defined as equation (3) according to Fujita's free volume theory [31], which is an extension of the Cohen-Turnbull theory. $A_d$ and $B_d$ in equation (3) are constants related to the shape and size of diffused penetrant small molecules. Equation (3) shows that the diffusion coefficient increases as the free volume fraction increases, and the diffusion coefficient decreases as the size of the penetrant small molecule increase. Kanehashi et al. [47], Hellums et al. [48], Hagg et al. [49], and McHattie et al. [50] reported the relationship in which the diffusion coefficient increases as the free volume fraction of various glassy polymers increases, and the diffusion coefficient decreases as the size of the permeable small molecule increases.

The gas permeability coefficient, $P$, is also described as the following function by applying equation (33).

$$P = RTA_p exp(-B_p / FFV) \tag{33}$$

where $A_p$ and $B_p$ are constants that depend on temperature and type of penetrant small molecules. This formula is quoted by Park and Paul [28], Kanehashi et al. [47], Aguilar-Vega and Paul [51], Aitken et al. [52], and McHattie et al. [53]. They explained the gas permeability of polymers in the glass state.

This study focuses on equation (33). According to each author's ideas, the hydrogen permeability coefficient ($P_a$) and $FFV_a$ can be expressed by equation (34).

$$P_a = RTA_p exp(-B_p / FFV_a) \tag{34}$$

In the amorphous region, the hydrogen permeability coefficients at high pressure and 0.6 MPa are $P_a^{HP}$ and $P_a^{0.6MPa}$, respectively. The FFV at 0.6 MPa and high pressure are $FFV_a^{0.6MPa}$ and $FFV_a^{HP}$, respectively. Equation (34) can be converted to equation (35) as follows:

$$P_a^{HP} = P_a^{0.6MPa} exp\left(\frac{B_p}{FFV_a^{0.6MPa}} - \frac{B_p}{FFV_a^{HP}}\right) \tag{35}$$

In the aforementioned hypothesis, it was mentioned that FFV decreases with hydrostatic pressure. The specific volume ($v_{specimen}$) of the specimen decreases due to pressure in the PVT measurement in Fig. 3.

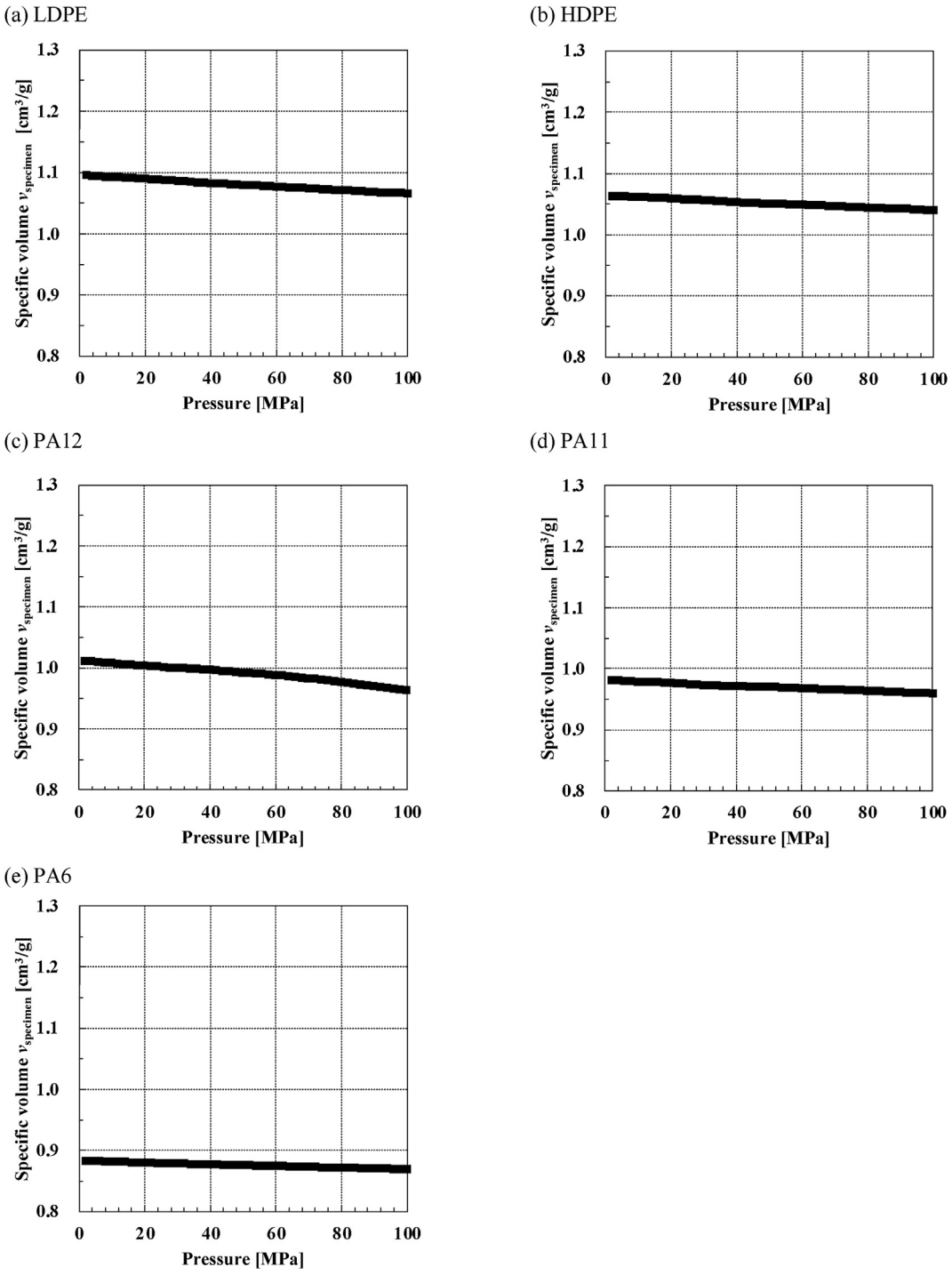


**Fig. 3 – Relationship between pressure and specific volume measured by PVT measurement. (a) LDPE, (b) HDPE, (c) PA12, (d) PA11, and (e) PA6.**

To calculate the compression of free volume in the amorphous region, the specific volume of the amorphous region is calculated using equation (36), assuming that the degree of crystallinity does not change with hydrostatic pressure. From the aforementioned statements, the $FFV_a$ can be derived from equation (30).

$$\rho_a = \rho\rho_C(1-\chi_C)/(\rho_c-\rho\chi_C) \tag{36}$$

Fig. 4 shows the pressure dependency of $FFV$ and $FFV_a$. Both decrease as the pressure increases. The $FFV$ was compressed by hydrostatic pressure.

Table 6 and Fig. 5 show the relationship between the reciprocal of the free volume fraction ($1/FFV_a^{0.6MPa}$) and the permeation coefficient ($P_a^{0.6MPa}$) in the amorphous region at 0.6 MPa. The free volume fraction correlates with the amount of diffusion and permeation through molecular chain

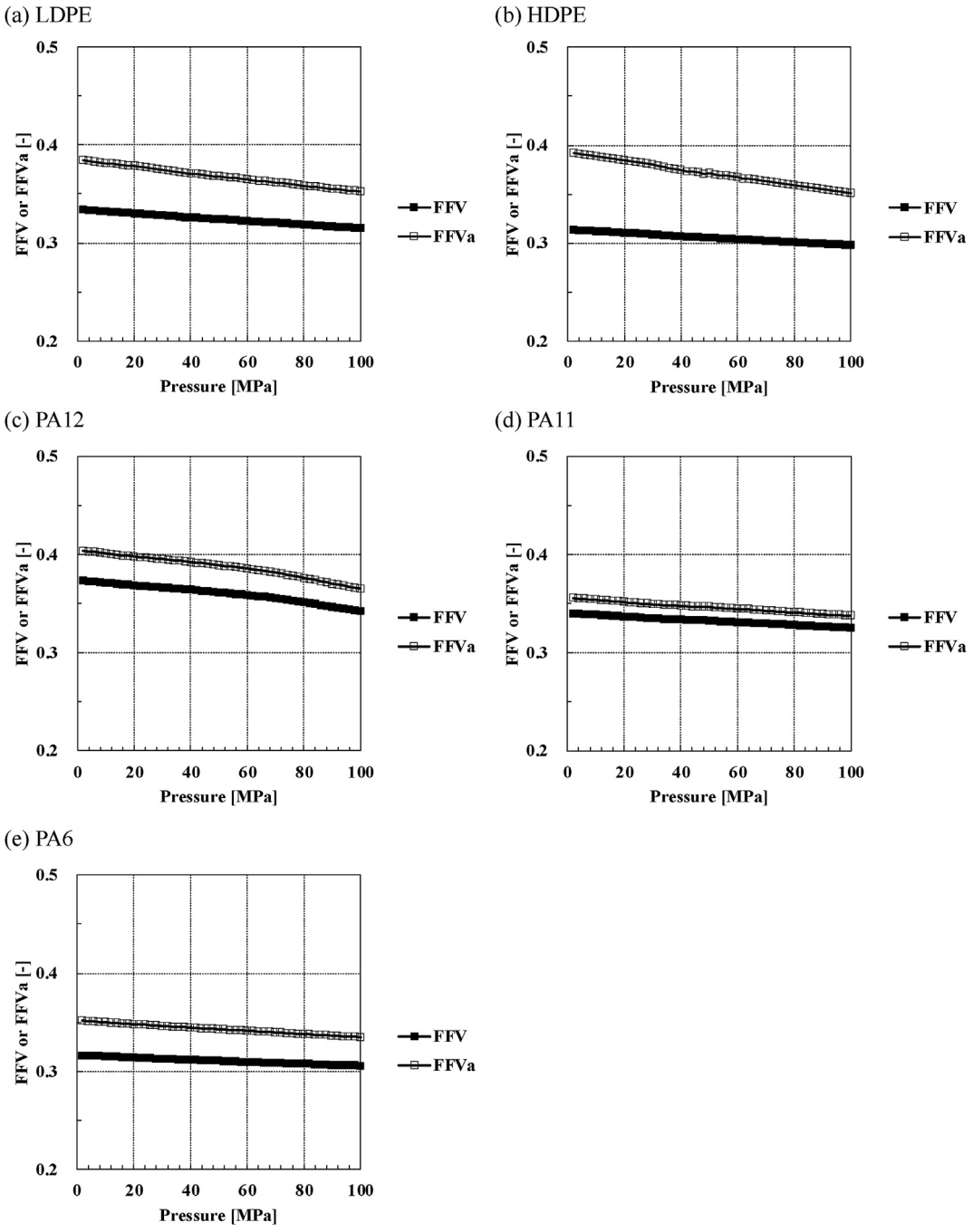


**Fig. 4 – *FFV* and $FFV_a$ dependence on hydrogen pressure.**

mobility. $B_p$ in equation (34) is a constant related to the shape and size of the penetrant gas molecules diffused in the polymer matrix. This parameter can be determined as the exponential term in Fig. 5, resulting in $B_p = 5.728$.

Using the permeation coefficient measured at low pressure, such as 0.6 MPa, *FFV* at low pressure and a target pressure, which can be determined by density measurement data and PVT measurement data of the material, equation (37) can be used to calculate the hydrogen permeation coefficient of the amorphous region ($P_a^{HP}$) in a high-pressure environment. The required data is obtained by the conventional experimental method. Finally, on the basis of equation (8), equation (37) can be used to calculate the permeation coefficient of the bulk crystalline polymer ($P_{Estimated}$) using the obtained $P_a^{HP}$ value and the volume fraction of the crystalline region ($\varphi_c$) and the length ($L_c$) and thickness ($W_c$) of crystallites.

$$P_{Estimated} = \left[\frac{1-\varphi_c}{1+\left(\frac{L_c}{2W_c}\right)\varphi_c}\right] P_a^{HP} \tag{37}$$

**Table 6 – Relationship between the reciprocal of the free volume fraction, $1/FFV_a^{0.6MPa}$, and the permeation coefficient, $P_a^{0.6MPa}$, in the amorphous region at 0.6 MPa.**

| Parameter | Bulk permeability | Amorphous free volume | Amorphous permeability |
|---|---|---|---|
| Symbol | $P^{0.6MPa}$ | $1/FFV_a^{0.6MPa}$ | $P_a^{0.6MPa}$ |
| Unit | $cm^3$(STP) cm /($cm^2$ s cmHg) | – | $cm^3$(STP) cm /($cm^2$ s cmHg) |
| EPDM | 5.00E-09 | 2.311 | 5.00E-09 |
| LDPE | 9.12E-10 | 2.640 | 1.86E-09 |
| HDPE | 4.34E-10 | 2.574 | 1.95E-09 |
| PA12 | 2.60E-10 | 2.472 | 3.63E-10 |
| PA11 | 2.10E-10 | 2.809 | 3.02E-10 |
| PA6 | 4.36E-11 | 2.840 | 8.26E-11 |

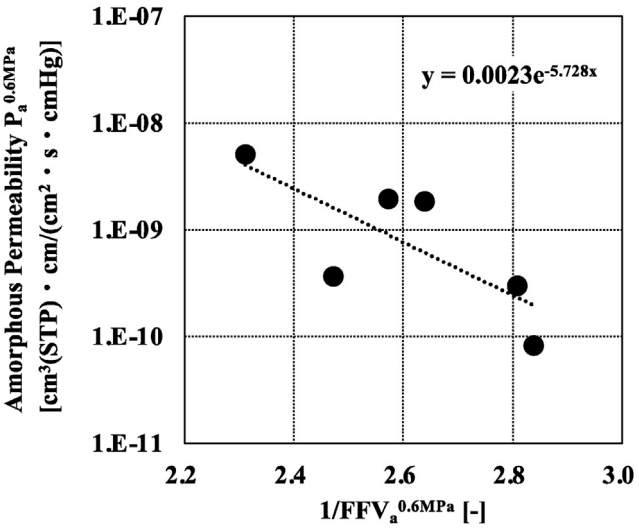


**Fig. 5 – The relationship between the reciprocal of free volume fraction $1/FFV_a^{0.6MPa}$ and the permeation coefficient $P_a^{0.6MPa}$ in the amorphous region at 0.6 MPa.**

### *Validation of the estimated hydrogen permeability coefficient in a high-pressure environment*

The validation of the hydrogen permeability coefficient ($P_{Estimated}$) in the high-pressure environment predicted by equation (37) was verified by comparing the experimental values of both the TDA and HPHP for the LDPE, HDPE, and PA11.

The results in Section 4.4 show that the pressure dependency of the hydrogen permeability coefficient in the amorphous region for LDPE, HDPE, and PA11 can be obtained from equation (35). Fig. 6 shows the pressure dependence of the permeability coefficient in the amorphous region. The free volume in the amorphous region is compressed as the pressure increases. Thus, the diffusivity decreases in a high-pressure hydrogen environment due to a decrease in FFV.

Table 7 and Fig. 7 <1> show the comparison between the hydrogen permeation coefficients of LDPE, HDPE, and PA11 estimated from equation (36) ($P_{Estimated}$) and the experimental values($P_{TDA}$) using the TDA method. Table 8 and Fig. 7 <2> show the comparison with the experimental values ($P_{HPHP}$) using the HPHP method.

Fig. 7 <2> shows the comparison between the estimated value ($P_{Estimated}$) and the experimental value ($P_{HPHP}$) of the permeation coefficient in a high-pressure hydrogen environment. Comparing the estimated value from equation (37) ($P_{Estimated}$) to the experimental value obtained by TDA ($P_{TDA}$), the experimental value ($P_{TDA}$) deviates significantly from the estimated value ($P_{Estimated}$) as the hydrogen pressure increases. For LDPE, the error increases with the hydrogen pressure, and an error ($P_{TDA}/P_{Estimated}$) of 17.1 times occurs between them at 90 MPa. In Fig. 7 <1>, two sets of data deviate significantly from one another. HDPE and PA11 errors are smaller than LDPE errors. The error tends to increase based on the hydrogen pressure.

By comparing the estimated values from equation (37) ($P_{Estimated}$) to the experimental values obtained by HPHP ($P_{HPHP}$), the error was smaller than that of the TDA method. The maximum error ($P_{HPHP}/P_{Estimated}$) was about 1.2 times.

The experimental values ($P_{TDA}$) obtained using the TDA method are derived from the product of the hydrogen solubility coefficient calculated from the amount of hydrogen dissolved in the high-pressure state estimated from the hydrogen diffusion behavior and the diffusion coefficient obtained from the diffusion behavior after opening the atmospheric pressure.

The crystalline-polymer specimen for TDA measurement is exposed to hydrostatic hydrogen pressure until it is saturated with hydrogen. The crystalline polymer specimen's free volume is compressed during the high-pressure hydrogen exposure; however, the TDA measurement is conducted at atmospheric pressure. Its free volume becomes larger than its pressurized state. Comparing the diffusion coefficients of the TDA method with the HPHP method, the TDA method has a faster hydrogen diffusion rate. Because the TDA measurement is conducted at atmospheric pressure, the free volume becomes the atmospheric pressure state; it makes sense that the diffusion coefficient of hydrogen in the polymer is larger than that in the HPHP method in which the free volume is compressed by the applied high-pressure hydrogen during measurement. According to the PVT measurement, the observed bulk-volume change compresses the free volume in the crystalline polymer specimen as the pressure increases. The diffusion and permeation of hydrogen are controlled by the $FFV_a$ originating from free volume compression, which reduces the FFV value.

The hydrogen permeation coefficient ($P_{HPHP}$) obtained using the HPHP method is calculated from equation (20) by measuring the amount of permeation from the high-pressure side to the low-pressure side of the polymer film under steady-state; therefore, high-pressure hydrogen is applied to the polymer film during the measurement. In terms of the free volume behavior, in the case of the HPHP method in which hydrostatic pressure is always applied and the free volume is compressed according to the pressure, the diffusion coefficient obtained by the HPHP method is estimated to be lower than that of the TDA method. It is considered that the pressure dependency is well reproduced in this estimated result since the result of the steady-state permeation test at low

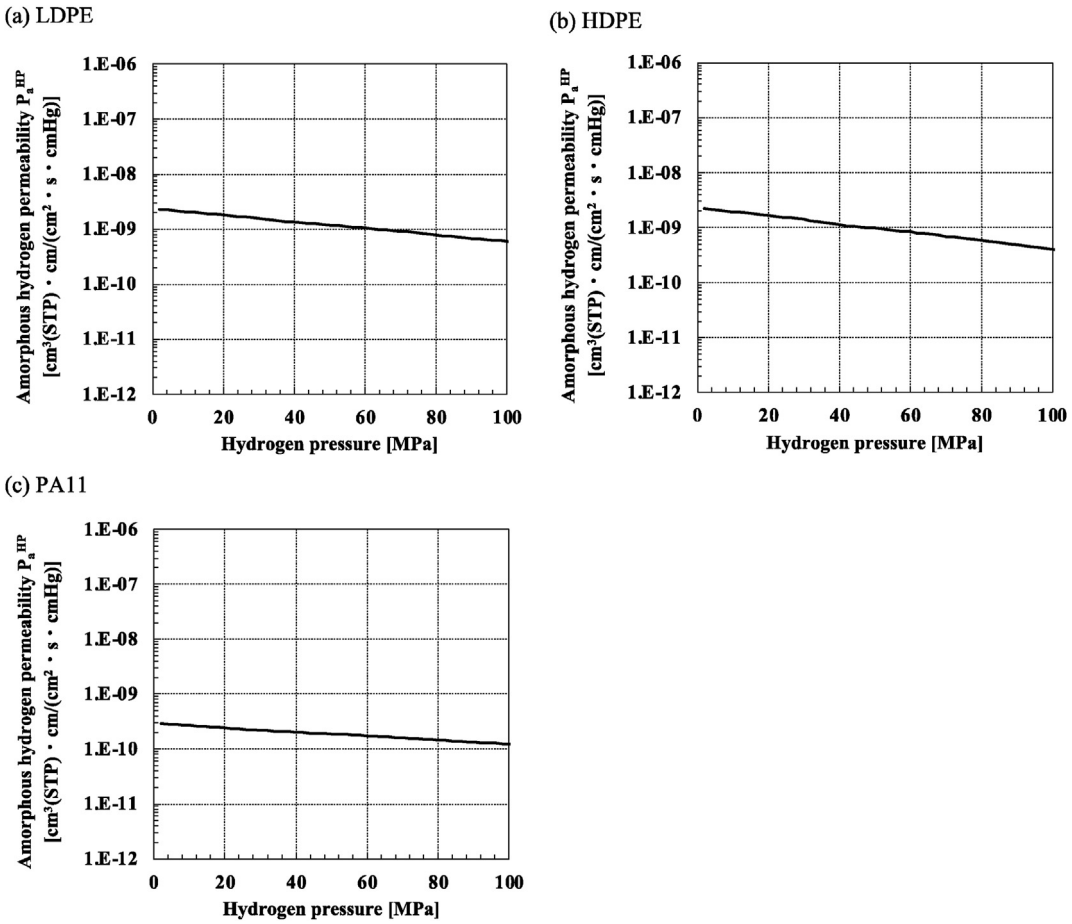


**Fig. 6 – Relationship between hydrogen pressure and $P_a^{HP}$**

**Table 7 – Comparison of the estimated value by equation (37) ($P_{Estimated}$) with TDA ($P_{TDA}$) in the hydrogen permeability coefficient.**

| Parameter | Pressure | Estimated value by equation (37) | TDA method | | | | | | | Error |
|---|---|---|---|---|---|---|---|---|---|---|
| | | Permeability | Hydrogen Content | Hydrogen density | Specific volume | Hydrogen Content | Solubility | Diffusion | Permeability | |
| Symbol | p | $P_{Estimated}$ | $C_0^H$ | $\rho_{Hydrogen}$ | $v_{specimen}$ | $V_{Hydrogen}$ | S | D | $P_{TDA}$ | $P_{TDA}/P_{Estimated}$ |
| Unit | MPa | cm³(STP) · cm/(cm² · s · cmHg) | μg/1g specimen | kg/m³ | cm³/g | mol/m³-specimen | mol/(m³ · Pa) | mm²/s | cm³(STP) · cm/(cm² · s · cmHg) | – |
| LDPE | 10 | 9.99E-10 | 230 | 8.00E+00 | 1.092 | 1.18E+00 | 1.16E-05 | 4.10E-04 | 1.42E-09 | 1.4 |
| | 30 | 7.77E-10 | 419 | 2.40E+01 | 1.085 | 7.18E-01 | 7.09E-06 | 2.60E-04 | 5.50E-10 | 0.7 |
| | 50 | 6.13E-10 | 462 | 4.00E+01 | 1.079 | 4.78E-01 | 4.72E-06 | 3.90E-04 | 5.49E-10 | 0.9 |
| | 70 | 4.85E-10 | 1352 | 5.60E+01 | 1.073 | 1.00E+00 | 9.91E-06 | 9.90E-04 | 2.93E-09 | 6.0 |
| | 90 | 3.75E-10 | 2334 | 7.20E+01 | 1.067 | 1.36E+00 | 1.34E-05 | 1.60E-03 | 6.39E-09 | 17.1 |
| HDPE | 10 | 4.33E-10 | 130 | 8.00E+00 | 1.061 | 6.84E-01 | 6.75E-06 | 2.00E-04 | 4.03E-10 | 0.9 |
| | 30 | 3.13E-10 | 394 | 2.40E+01 | 1.056 | 6.94E-01 | 6.85E-06 | 2.10E-04 | 4.30E-10 | 1.4 |
| | 50 | 2.13E-10 | 617 | 4.00E+01 | 1.050 | 6.56E-01 | 6.47E-06 | 1.90E-04 | 3.67E-10 | 1.7 |
| | 70 | 1.49E-10 | 711 | 5.60E+01 | 1.046 | 5.42E-01 | 5.35E-06 | 1.30E-04 | 2.08E-10 | 1.4 |
| | 90 | 1.26E-10 | 999 | 7.20E+01 | 1.041 | 5.95E-01 | 5.87E-06 | 1.40E-04 | 2.45E-10 | 2.0 |
| PA11 | 10 | 1.87E-10 | 122 | 8.00E+00 | 0.979 | 6.96E-01 | 6.87E-06 | 9.85E-05 | 2.02E-10 | 1.1 |
| | 30 | 1.51E-10 | 347 | 2.40E+01 | 0.973 | 6.63E-01 | 6.55E-06 | 1.04E-04 | 2.03E-10 | 1.3 |
| | 50 | 1.32E-10 | 571 | 4.00E+01 | 0.970 | 6.57E-01 | 6.49E-06 | 1.13E-04 | 2.19E-10 | 1.7 |
| | 70 | 1.11E-10 | 745 | 5.60E+01 | 0.966 | 6.15E-01 | 6.07E-06 | 1.30E-04 | 2.36E-10 | 2.1 |
| | 90 | 9.25E-11 | 1057 | 7.20E+01 | 0.961 | 6.82E-01 | 6.73E-06 | 1.24E-04 | 2.49E-10 | 2.7 |

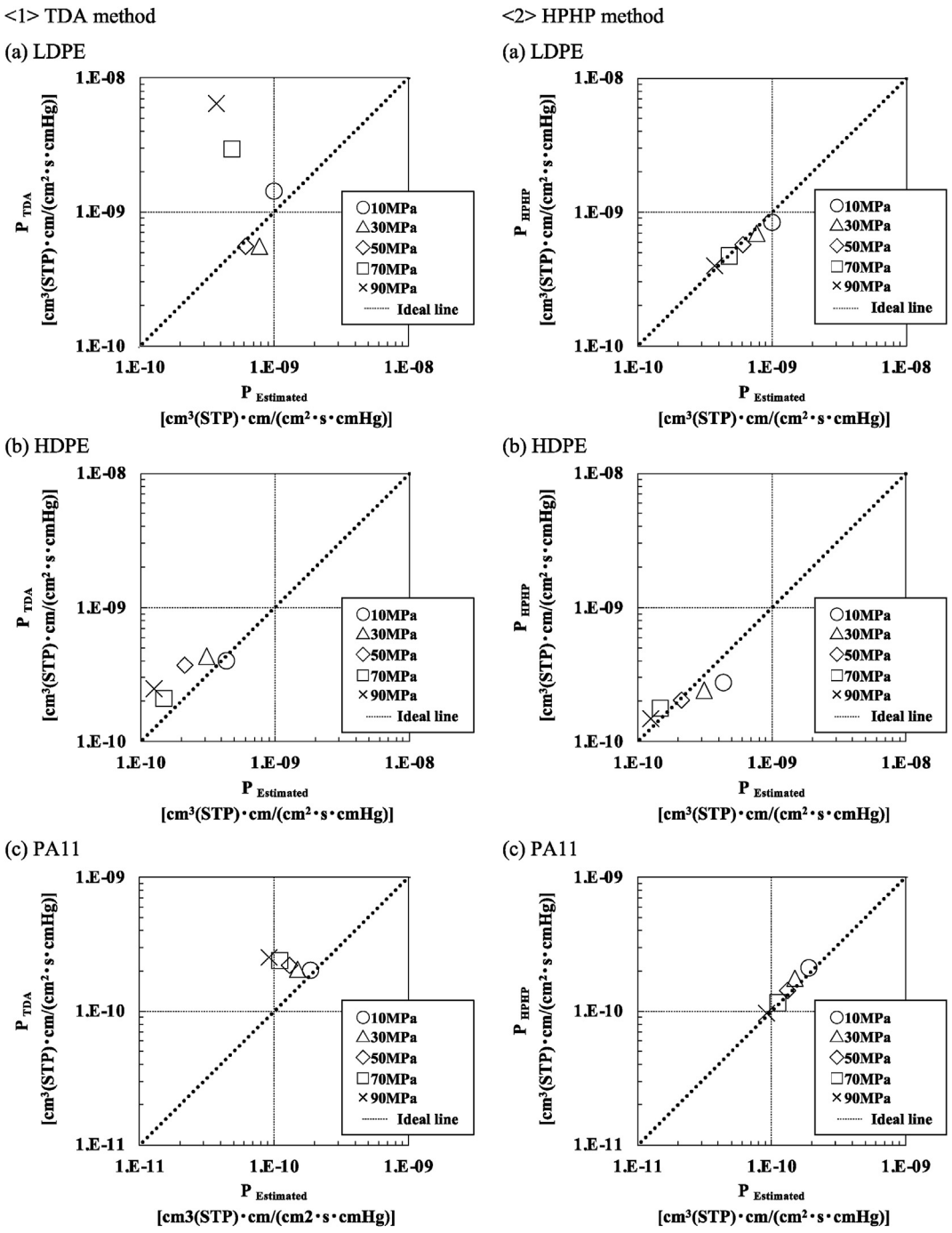


**Fig. 7 – Comparison of the estimated value by equation (37) ($P_{Estimated}$) with the TDA method ($P_{TDA}$) and HPHP method ($P_{HPHP}$) in the hydrogen permeability coefficient.**

pressure (0.6 MPa) was corrected by estimating the decrease in free volume by the PVT test. The proposed permeation model can be used to estimate the hydrogen permeation behavior for crystalline polymers in the HPHP method. The hydrogen permeation coefficient derived using the HPHP method can be predicted using equation (37).

The bulk modulus of LDPE, HDPE, and PA11 calculated by PVT measurements are 4497, 5010, and 4568 MPa, respectively. LDPE, which has a low degree of crystallinity and a low compression modulus, has the highest effect of free volume compression under hydrostatic pressure. In addition, LDPE has the largest amount of dissolved hydrogen obtained from TDA measurement due to its low crystallinity and has a high diffusion coefficient due to the influence of the free volume recovered after depressurization to the atmospheric pressure. This is a factor that increases the error in TDA measurement prediction results.

The permeation model described in Section 4.4 can explain the hydrogen permeation behavior of crystalline polymers during the HPHP measurement. Equation (37) can be used to

**Table 8 – Comparison of the estimated value by equation (37) ($P_{Estimated}$) with the HPHP method ($P_{HPHP}$) in hydrogen permeability coefficient.**

| Parameter | Pressure | Estimated value by equation (37) | HPHP method | | | Error |
|---|---|---|---|---|---|---|
| | | Permeability | Diffusion | Solubility | Permeability | |
| Symbol | p | $P_{Estimated}$ | D | S | $P_{HPHP}$ | $P_{HPHP}/P_{Estimated}$ |
| Unit | MPa | $cm^3(STP) \cdot cm/(cm^2 \cdot s \cdot cmHg)$ | $mm^2/s$ | $mol/(m^3 \cdot Pa)$ | $cm^3(STP) \cdot cm/(cm^2 \cdot s \cdot cmHg)$ | – |
| LDPE | 10 | 9.99E-10 | 3.18E-04 | 8.92E-06 | 8.46E-10 | 0.8 |
| | 30 | 7.77E-10 | 2.65E-04 | 8.77E-06 | 6.94E-10 | 0.9 |
| | 50 | 6.13E-10 | 2.29E-04 | 8.29E-06 | 5.67E-10 | 0.9 |
| | 70 | 4.85E-10 | 1.99E-04 | 7.86E-06 | 4.67E-10 | 1.0 |
| | 90 | 3.75E-10 | 1.82E-04 | 7.30E-06 | 3.96E-10 | 1.1 |
| HDPE | 10 | 4.33E-10 | 1.35E-04 | 6.85E-06 | 2.76E-10 | 0.6 |
| | 30 | 3.13E-10 | 1.28E-04 | 6.29E-06 | 2.40E-10 | 0.8 |
| | 50 | 2.13E-10 | 1.08E-04 | 6.26E-06 | 2.02E-10 | 0.9 |
| | 70 | 1.49E-10 | 9.90E-05 | 5.95E-06 | 1.76E-10 | 1.2 |
| | 90 | 1.26E-10 | 8.40E-05 | 5.87E-06 | 1.47E-10 | 1.2 |
| PA11 | 10 | 1.87E-10 | 5.20E-05 | 1.36E-05 | 2.10E-10 | 1.1 |
| | 30 | 1.51E-10 | 6.35E-05 | 9.26E-06 | 1.76E-10 | 1.2 |
| | 50 | 1.32E-10 | 5.55E-05 | 8.53E-06 | 1.41E-10 | 1.1 |
| | 70 | 1.11E-10 | 4.78E-05 | 8.03E-06 | 1.15E-10 | 1.0 |
| | 90 | 9.25E-11 | 4.26E-05 | 7.54E-06 | 9.58E-11 | 1.0 |

predict the hydrogen permeation coefficient derived using the HPHP method.

## Conclusions

In this study, we measured the pressure dependency of the hydrogen permeability of crystalline polymers, such as low-density polyethylene (LDPE), high-density polyethylene (HDPE), and polyamide 11 (PA11). According to the high-pressure hydrogen permeation (HPHP) method results, the hydrogen permeation coefficient at a pressure of 90 MPa is about 0.3–0.4 times lower than that at a pressure of 0.6 MPa. To clarify the phenomena, the hydrogen permeability of the crystalline polymer under high pressure was estimated using a Nielsen model in which the crystalittes in the polymer are regarded as fillers. We constructed the permeation model for crystalline polymers in terms of the tortuosity induced by their higher-order structures and free volume change in the amorphous region evaluated using PVT method for measuring the relationship between pressure (p), specific volume (v) and temperature (T) in the molten-solid state of a polymer. The results of the pressure dependency of hydrogen permeability were reproduced by the developed permeation model. The proposed model is applied to polymers with different crystallinities produced by molding methods such as injection, extrusion, blow molding, etc., and may lead to the development of simple and useful design and evaluation methods for polymer inner layers used in compressed hydrogen storage and transfer equipment.

## Declaration of competing interest

The authors declare that they have no known competing financial interests or personal relationships that could have appeared to influence the work reported in this paper.

## Acknowledgments

The authors acknowledge many supports from the members of Hydrogen Polymers Division, Research Center for Hydrogen Industrial Use and Storage (HYDROGENIUS), Kyushu University.

## REFERENCES

[1] National greenhouse gas Inventory report of Japan, Ministry of the environment, Japan, greenhouse gas Inventory Office of Japan (GIO), CGER. NIES 2021;2–5.
[2] The Ministry of Land, Infrastructure. Transport and Tourism in Japan. https://www.mlit.go.jp/sogoseisaku/environment/sosei_environment_tk_000007.html; 2021.
[3] Berens AR, Hopfenberg HB. J Membr Sci 1982;10:283–303.
[4] Valappil RSK, Ghasem N, Al-Marzouqi M. Current and future trends in polymer membrane-based gas separation technology: a comprehensive review. J Ind Eng Chem 2021;98:103–29.
[5] Cui Z, Drioli E, Lee YM. Recent progress in fluoropolymers for membranes. Prog Polym Sci 2014;39:164–98.
[6] Merkel TC, Pinnau I, Prabhakar RS, Freeman BD. Gas and vapor transport properties of perfluoropolymers. In: Freeman BD, Yampolskii YP, Pinnau I, editors. Materials science of membranes for gas and vapor separation. New York, NY, USA: Wiley; 2006. p. 251–70.
[7] Tanihara N, Kusuki Y. Gas and vapor separation by polyimide membrane. Kagaku Kogyo 1996;70:160.
[8] Matsui S, Sato H, Nakagawa T. Effects of low molecular weight photosensitizer and UV irradiation on gas permeability and selectivity of polyimide membrane. J Membr Sci 1998;141:31.
[9] Chen WJ, Martin CR. Gas-transport properties of sulfonated polystyrenes. J Membr Sci 1994;95:51–61.
[10] Kocha SS, Yang JD, Yi JS. Characterization of gas crossover and its implications in PEM fuel cells. AIChE J 2006;52:1916–25.
[11] Yasuda H, Rosengren Kj. J Appl Polym Sci 1970;14:2839.
[12] Salame M. J Polym Sci Symp 1973;41:1.

[13] Miyake H, Matsuyama H, Ashida K, Watanabe K. J. Vac. Sci. Technol. A- 1983;1(3):1447.
[14] Michaels AS, Bixler HJ. J. Polym. Science 1961;50:413.
[15] Myers AW, Stannett V, Szwarc M. J Polym Sci 1959;35:285.
[16] Tikhomirov BP, Hopfenberg HB, Stannett VT, Williams JL. Makromol Chem 1968;118:177.
[17] Chiou JS, Paul DR. J. Appl. Polym. Science 1987;34:1037.
[18] Waack R, Alex NH, Frisch HL, Stannett V, Szwarc M. Ind Eng Chem 1955;47:2524.
[19] Ito Y. Kobunshi Kagaku 1961;18:124.
[20] Simril VL, Hershberger A. Mod Plast 1950;27(11):95.
[21] Ito Y. Kobunshi Kagaku 1961;18:158.
[22] Klopffer M, Berne P, Espuche É. Development of Innovating materials for distributing mixtures of hydrogen and Natural gas. Study of the barrier properties and Durability of polymer Pipes. Oil & Gas Science and Technology–Rev. IFP Energies Nouvelles 2015;70(No. 2):305–15.
[23] Sun Y, Lv H, Zhou W, Zhang CM. Research on hydrogen permeability of polyamide 6 as the liner material for type IV hydrogen storage tank. Int J Hydrogen Energy 2020;45:24980–90.
[24] Shibutani M. Development of high-pressure hydrogen gas barrier material. Journal of the Rubber Society of Japan 2015;88(8):336–41.
[25] Salame M. Prediction of gas barrier properties of high polymers. Polym Eng Sci 1986;26:1543–6.
[26] Bicerano J. Prediction of polymer properties. New York: Marcel Dekker; 1993.
[27] Lee KH, Hwang ST. The transport of Condensible Vapors through a Microporous Vycor glass membrane. J Colloid Interface Sci 1986;110:544–55.
[28] Park JY, Paul DR. Correlation and prediction of gas permeability in glassy polymer membrane materials via a modified free volume based group contribution method. J Membr Sci 1997;125:23–39.
[29] Cohen MH, Turnbell D. Molecular transport in Liquids and glasses. J Membr Sci 1982;10:283.
[30] Fujita H. Diffusion in polymer-Diluent systems. Fortschr Hochpolym-Forsch 1961;3:1–47.
[31] Fujiwara H, Ono H, Onoue K, Nishimura S. High-pressure gaseous hydrogen permeation test method -property of polymeric materials for high- pressure hydrogen devices (1). Int J Hydrogen Energy 2020;45:29082–94.
[32] Fujiwara H, Ono H, Ohyama K, Kasai M, Kaneko F, Nishimura S. Hydrogen permeation under high pressure conditions and the destruction of exposed polyethylene-property of polymeric materials for high-pressure hydrogen devices (2). Int J Hydrogen Energy 2021;46:11832–48.
[33] Michael AS, Bixler HJ. Flow of gases through polyethylene. J Polym Sci 1961:413–39.
[34] Wang Y, Easteal AJ, Dong Chen X. Ethylene and Oxygen permeability through polyethylene Packaging films. Packag Technol Sci 1998;11:169–78.
[35] Nagai K. Barrier technology. Kyoritsu Shuppan Co., Ltd.; 2014. p. 79.
[36] Maxwell JC. A treatise on Electricity and Magnetism. NewYork: Dover Publications; 1954.
[37] Nielsen LE. Models for the permeability of filled polymer systems. J Macromol Sci 1967;A1(5):929–42.
[38] Matsuo M, Sawatari C. Elastic modulus of polyethylene in the crystal chain direction as measured by X-ray diffraction. Macromolecules 1986;19:2036–40.
[39] Kaji K, Sakurada I. Determination of the elastic modulus of polyamide crystals along the chain Axis by X-ray diffraction, 1. Makromol Chem 1978;179:209–17.
[40] Verma P, Kumar A, Chauhan SS, Verma M, Malik RS, Choundhary V. Industrially viable technique for the preparation of HDPE/fly ash composites at high loading: thermal, mechanical, and rheological interpretations. J Appl Polym Sci 2018;10:45995.
[41] Liao G, Li Z, Cheng Y, Xu D, Zhu D, Jiang S. Properties of oriented carbon fiber/polyamide 12 composite parts fabricated by fused deposition modeling. Mater Des 2017;139:283–92.
[42] Ruehle DA, Perbix C, Castañeda M, Dorgan JR, Mittal V, Halley P, Martin D. Blends of biorenewable polyamide-11 and polyamide-6,10. Polymer 2013;54:6961–70.
[43] Millot C, Fillot LA, Lame O, Sotta P, Seguela R. Assessment of polyamide-6 crystallinity by DSC. J Therm Anal Calorim 2015;122:307–14.
[44] Strobl GR. Polymer Physics. Maruzen publishing; 2010. p. 169–71.
[45] Yamabe J, Nishimura S. Influence of fillers on hydrogen penetration properties and blister fracture of rubber composites for O-ring exposed to high-pressure hydrogen gas. Int J Hydrogen Energy 2009;34(4):1977–89.
[46] van Krevelen DW, te Nijenhuis K. Properties of Polymers Fourth, completely revised edition. ELSEVIER; 2009. p. 920–1.
[47] Kanehashi S, Nagai K. Analysis of dual-mode model parameters for gas sorption in glassy polymers. J Membr Sci 2005;253:117–38.
[48] Hellums MW, Koros WJ, Schmidhauser JC. Gas separation properties of spirobiindane polycarbonate. J. Membr. Science 1992;67:75–81.
[49] Hagg M-B, Koros WJ, Schmidhauser JC. Gas sorption and transport properties of bisphenol-I-polycarbonate. J Polym Sci, Part B: Polym Phys 1994;32:1625–33.
[50] McHattie JS, Koros WJ, Paul DR. Gas transport properties of polysulphones. 1. Role of symmetry of methyl group placement on bisphenol rings. Polymer 1991;32:840–50.
[51] Aguilar-Vega M, Paul DR. Gas transport properties of polycarbonates and polysulfones with aromatic substitutions on the bisphenol connector group. J Polym Sci, Part B: Polym Phys 1993;31:1599–610.
[52] Aitken CL, Koros WJ, Paul DR. Effect of structural symmetry on gas transport properties of polysulfones. Macromolecules 1992;25:3424–34.
[53] McHattie JS, Koros WJ, Paul DR. Gas transport properties of polysulphones. 3. Comparison of tetramethyl-substituted bisphenols. Polymer 1992;33:1701–11.